ISSN 1063-7737, Astronomy Letters, 2009, Vol. 35, No. 2, pp. 75–86. © Pleiades Publishing, Inc., 2009.
Original Russian Text © O.K. Sil'chenko, I.V. Chilingarian, V.L. Afanasiev, 2009, published in Pis'ma v Astronomicheskiĭ Zhurnal, 2009, Vol. 35, No. 2, pp. 87–99.

Star Formation History in the Central Region of the Barred Galaxy NGC 4245

O. K. Sil'chenko[1*], I. V. Chilingarian[1,2], and V. L. Afanasiev[3]

[1] *Sternberg Astronomical Institute, Universitetskii pr. 13, Moscow, 119992 Russia*

[2] *Observatoire de Paris-Meudon, Laboratoire d'Etude du Rayonnement et de la Matiere en Astrophysique, 61 Av. de l'Observatoire, Paris, 75014 France*

[3] *Special Astrophysical Observatory, Russian Academy of Sciences, Nizhnii Arkhyz, 369167 Karachai-Cherkessian Republic, Russia*

Received May 26, 2008

Abstract—We have investigated the gas and stellar kinematics and the stellar population properties at the center of the early-type galaxy NGC 4245 with a large-scale bar by the method of two-dimensional spectroscopy. The galaxy has been found to possess a pronounced chemically decoupled compact stellar nucleus, which is at least a factor of 2.5 richer in metals than the stellar population of the bulge, and a ring of young stars with a radius of 300 pc. Star formation goes on in the ring even now; its location corresponds to the inner Lindblad resonance of the large-scale bar. According to Hubble Space Telescope data, the mean stellar age in the chemically decoupled nucleus is significantly younger than that within $0''.25$ of the center. It may be concluded that we take the former ultracompact star formation ring with a radius of no more than 100 pc located at the inner Lindblad resonance of the now disappeared nuclear bar as the chemically decoupled nucleus. On the whole, the picture of star formation at the center of this gas-poor galaxy is consistent with theoretical predictions of the consequences of the secular evolution of a stellar–gaseous disk under the action of a bar or bars.

PACS numbers : 98.52.Lp; 98.58.Ay; 98.62.Ai; 98.62.Hr; 98.62.Js; 98.62.Lv; 98.62.Bj
DOI: 10.1134/S1063773709020029

Key words: *galactic nuclei, galactic structure, galactic evolution.*

INTRODUCTION

The mechanisms of the so-called secular evolution, the slow rearrangement accompanied by starbursts in special places (for more details on secular evolution, see the review by Kormendy and Kennicutt (2004)), play a major role in the lives of disk galaxies. On long time scales, secular evolution can result in a change of the galaxy's morphological type; for example, the (trans)formation of lenticular galaxies from spiral ones is probably an example of secular evolution. The mechanisms of secular evolution that are now suggested by theorists can be roughly divided into external and internal ones. The internal mechanisms are those that will act even if the galaxy is left alone in absolute solitude; these primarily include the various dynamical instabilities of stellar–gaseous disks, in particular, those that lead to the formation of bars. However, the formation of a bar at the dist center can also be provoked by an external tidal impact. The external mechanisms of secular evolution can be divided, again roughly, into gravitational and gasdynamic ones. The former include the encounters and gravitational interactions of galaxies; the latter include the impact of a hot intracluster medium, which is present in large quantities in clusters and massive groups of galaxies, on the gaseous disks of galaxies.

The small early-type disk galaxy NGC 4245 (for its basic parameters, see the table) is a rich object for studying the consequences of the impact of various secular evolution mechanisms: it has an extended high-contrast ("strong") bar and it is located in the dense part of a nearby galaxy group, the Coma I Cloud. NGC 4245 is about 100 kpc away from the group center (NGC 4278) and the giant spiral galaxy NGC 4274 is even closer, at 59 kpc. Generally, the group is rather large, contains about twenty galaxies to an absolute magnitude of -16^m, and most of these galaxies are spiral (Gregory and Thompson 1977). Interestingly, the spiral galaxies of the Coma I Cloud located within the central half-megaparsec are poor in neutral hydrogen (Garcia-Barreto et al. 1994) and the bulk of their gas is in molecular form (Gerin and

*E-mail: olga@sai.msu.su

Global parameters of NGC 4245

Morphological type (NED[1])	SB(r)0/a
V_r (HYPERLEDA[2])	885 km s^{-1}
Distance (Gregory and Thompson 1977)	13 Mpc
D_{25} (RC3[3])	2.9′
R_{25}	5.5 kpc
B_T^0 (RC3)	12.01
$(B-V)_T^0$ (RC3)	0.86
$(U-B)_T^0$ (RC3)	0.44
M_B (HYPERLEDA)	-18.74
$V_{\max}$(H I), km s^{-1}	$94/\sin i$
Inclination (HYPERLEDA)	56°
$PA_{\rm phot}$ (HYPERLEDA)	146°

[1] NASA/IPAC Extragalactic Database.
[2] Lyon–Meudon Extragalactic Database.
[3] Third Reference Catalogue of Bright Galaxies.

Casoli 1994). For example, in NGC 4245, the H_2-to-H I ratio is 4 (in disk galaxies, this ratio is, on average, considerably smaller than unity). These peculiarities are usually typical of spiral galaxies in clusters (see, e.g., Sullivan and Johnson 1978; Solanes et al. 2001; Kenney and Young 1986) and are commonly explained by the interaction of a cold galactic gas with a hot intracluster gas: ram-pressure stripping of the tenuous HI gas from the galactic disk periphery can both reduce the HI content and increase the fraction of H_2, which is denser and collected in the central part of the galaxy. Interestingly, there is no hot X-ray gas in the Coma I Cloud (Mulchaey et al. 2003) and the HI deficiency in its spiral galaxies, no matter how closely it resembles that in the spiral galaxies of clusters, should be explained in a different way. Nothing but the gravitational interaction effects come into mind here. These effects should also provoke axial symmetry breaking in the disks (bar generation), noncircular gas motions, and central starbursts. Let us consider the star formation history at the center of NGC 4245—this may turn out to be a typical history for a disk galaxy at the center of a dense group.

OBSERVATIONS

The central region of NGC 4245 was observed with the Multi-Pupil Fiber Spectrograph (MPFS) mounted at the prime focus of the 6-m Special Astrophysical Observatory (SAO) telescope on the night from February 18 to February 19, 2007 (for a description of the instrument, see Afanasiev et al. 2001). The seeing (spatial resolution) estimated from the image of a standard star was about 2″.5. We used the blue–green spectral range 4200–5600 Å and the red range 5800–7200 Å with a reciprocal dispersion of 0.75 Å per pixel (a spectral resolution of about 3 Å). The detector was a 2048 × 2048-pixel CCD array. During MPFS observations, an array of densely packed square microlenses (16 × 16) forms a matrix of pupils that are transferred to the spectrograph slit via optical fibers. Such a configuration allows 256 spectra to be taken simultaneously in the full spectral range, each of which corresponds to a 1″.0 × 1″.0 square spatial image element of the galaxy. A separate bundle of optical fibers "brings" the emission from an empty night-sky field approximately ≈4′ away from the object being observed to the slit; the night-sky spectra are located on the CCD detector between the object spectra, are reduced together with the latter, and are then subtracted after the proper normalization. The comparison spectrum of a helium–neon–argon lamp is taken separately to calibrate the wavelength scale; the spectrum of a flat-field lamp and the dawn-sky spectrum are taken to correct the image for vignetting and different microlens passbands. The primary data reduction (bias subtraction, cosmic ray particle hit removal, extraction of the one-dimensional spectra from the CCD format, and linearization of the extracted spectra) was performed using a software package in the IDL programming environment (Afanasiev et al. 2001) modified to work with the absorption spectra of objects with low velocity dispersions (Chilingarian et al. 2007).

The MPFS observations in the range 4200–5600 Å were used to investigate the stellar kinematics (line-of-sight velocities and velocity dispersions) and to analyze the stellar population properties by two methods: (1) by measuring the absorption line equivalent widths expressed as Lick indices (Worthey et al. 1994) and (2) by directly fitting the galaxy spectra with model spectra of simple stellar populations (Chilingarian et al. 2007). The processed data cube was subjected to the procedure of adaptive Voronoi tesseleration (Cappellari and Copin 2003) to achieve a minimum signal-to-noise ratio of 20 in each bin. Subsequently, each spectrum was: (1) fitted with PEGASE.HR stellar population models (Le Borgne et al. 2004) to determine the line-of-sight velocities, velocity dispersions, ages, and metallicities; and (2) the absorption line indices Hβ, Mgb, Fe5270, and Fe5335 were calculated. Two-dimensional "maps" of kinematics, stellar population parameters, and Lick indices were then constructed from individual measurements. Since detailed calculations based on evolutionary synthesis models of an old stellar population exist for the indices of these strong lines

(see, e.g., Worthey 1994; Thomas et al. 2003), the mean stellar population parameters can be estimated by comparing the observed and model Lick indices.

For accurate measurements of kinematics, particularly at low velocity dispersions, the variations in MPFS spectral resolution over the field of view and over the spectral range should be taken into account by direct fitting. For this purpose, we directly fitted the dusk-sky spectrum observed on the same night and with the same instrumentation as the galaxy by the spectrum of the Sun (spectral type G2) from the ELODIE library of stellar spectra (Prugniel and Soubiran 2004) that has exactly the same spectral resolution as the PEGASE.HR models ($R = 10\,000$). Since the squares of the line widths are added in the operations with Gaussian profiles, the PEGASE.HR spectral resolution turns out to be "infinite" compared to the MPFS resolution ($R = 1300 \ldots 1800$), so that the achieved spectral resolutions closely match the spectrograph characteristics.

To analyze the ionized-gas kinematics, we used the spectra in the red range 5800–7200 Å containing emission lines of the ionized gas, with the strongest of them being Hα and [N II] λ6583. The line-of-sight velocities for the ionized gas were calculated from the positions of the emission line centroids.

We estimate the accuracy of the individual stellar line-of-sight velocity measurements as 5–7 km s^{-1} and the accuracy of determining the absorption line equivalent widths at the galactic center as 0.15 Å. The accuracy of the line-of-sight velocity estimates for the ionized gas is about 10 km s^{-1}. The accuracy of the spectrum linearization and the measured velocity zero point was checked using the night-sky [O I] λ5577 and λ6300 lines.

The galaxy NGC 4245 was also observed previously, on April 18, 2002, at the William Herschel 4.2-m telescope (La Palma) with the SAURON integral-field spectrograph. SAURON is an international project that includes three comanagers from France, the Netherland, and Great Britain and a number of European participants. A description of the spectrograph, the project, and the team can be found in Bacon et al. (2001). The principle of the spectrograph is based on the classical Courtes scheme of turning a lenslet array through a small angle relative to the direction of dispersion. This allows the spectra to be separated on the detector without optical fibers—the so-called "tiger mode." In SAURON, a medium-band interference filter cuts out a spectral range of approximately 4800–5400 Å; both the filter transmission curve (spectral range) and the reciprocal dispersion, which we estimated to be in the range 1.11–1.21 Å per pixel (spectral resolution about 4 Å), change over the field of view. The sky is exposed simultaneously with the object: it is observed only at 1.′7 from the center of the object under study and is transferred to the edge of the same lenslet array. On the night when NGC 4245 was observed, the average seeing that we estimated from ten stars observed before and after the galaxy observations was 1.″4. The completely processed cube of spectral data for NGC 4245 reduced to a spectral resolution of 108 km s^{-1} over the entire field of view was kindly provided us by J. Falcon-Barroso; a description of these data and the conclusions on the kinematics and the stellar population drawn from the calculation of absorption line indices and their comparison with stellar population models are contained in the papers of the SAURON team (Falcon-Barroso et al. 2006; Peletier et al. 2007).

THE KINEMATICS AND STRUCTURE OF THE CENTRAL PART OF NGC 4245

Figure 1 presents the results of our two-dimensional spectroscopy for the central region of NGC 4245 with the MPFS—the stellar and gas line-of-sight velocity maps, the stellar velocity dispersion map, and the Hα surface brightness distribution. We see a (circum)nuclear ring of ongoing star formation with a radius of 4″–6″ at the galactic center—here, the Hα emission intensity is at a maximum, while the Hα-to-[N II] λ6583 ratio exceeds 2 (Fig. 1d). The Hα emission intensity is distributed along the ring nonuniformly; two or, possibly, three knots (H II regions) where the star formation rate is particularly high are observed. This is not a rare occurrence in the nuclear star formation rings (see, e.g., Boker et al. 2008). The stellar velocity dispersion at the center of NGC 4245 is low everywhere, but it exhibits a minimum, about 60 km s^{-1}, at the very center. This can be interpreted as the presence of a compact, dynamically cold stellar disk at the very center (nucleus) of the galaxy. The stellar velocity dispersion increases approximately to 85 km s^{-1} at the edge of the field of view, at 8″–10″ from the nucleus—in this range of radii, we probably see the dynamically hotter stellar bulge of the galaxy. The line-of-sight velocity fields of both gas and stars appear as regular rotation. However, at low stellar velocity dispersion and inevitably small asymmetric drift, the stars for some reason rotate approximately a factor of 3 more slowly than the gas, although both components rotate in the same gravitational potential.

NGC 4245 is a galaxy with a large-scale bar. We analyzed the SSDS CCD images of the galaxy. The outermost isophotes, at $R > 50''$, allow the following orientation parameters of the galactic plane to be fixed by assuming a circular shape and a small

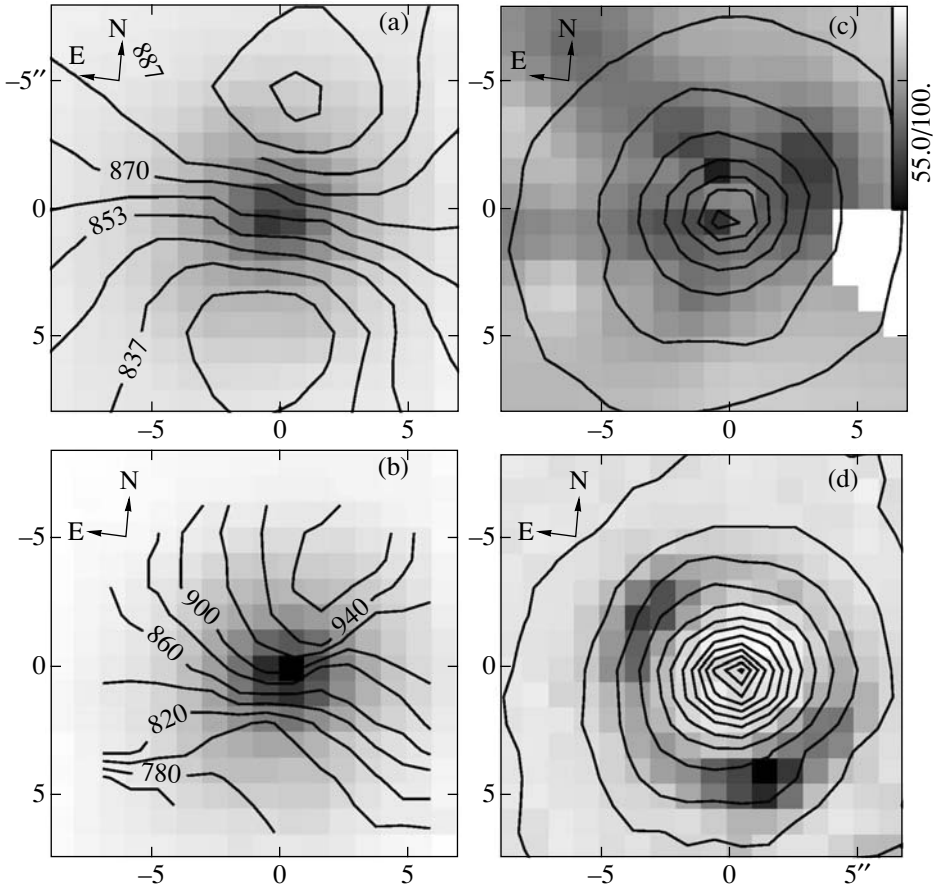

Fig. 1. Three kinematic maps for NGC 4245 and the distribution of ionized gas: (a) isovels of the stellar line-of-sight velocity field, (b) isovels of the ionized-gas line-of-sight velocity field, both against the background of the continuum intensity indicated by different shades of gray; (c) stellar velocity dispersion, km s^{-1}, (d) Hα emission line intensity, both are represented by different shades of gray; the isolines superimposed on the maps characterize the brightness distribution in continuum.

thickness of the outer disk: the inclination to the line of sight $i = 40°$ and the orientation of the line of nodes in the plane of the sky $PA_0 = 154°$. At a distance of $R = 35″$ from the center, the ellipticity of the isophotes reaches a maximum, while their orientation changes by $PA = 135°$—this is the region of the maximum photometric contribution from the bar. In a nonaxisymmetric potential, the kinematic major axis (the direction of the maximum line-of-sight velocity gradient) should turn relative to the line of nodes in the direction opposite to the turn of the bar isophotes (see, e.g., Moiseev and Mustsevoi 2000). In Fig. 2, we compare the orientations of the kinematic major axes of the gas and stellar velocity fields with the orientation of the isophotes based on SDSS and Hubble Space Telescope (HST) data and with the line of nodes of the global galactic plane. In the range of distances from the center $1″$–$3″$ (Fig. 2a) and at radii $R > 10″$ (Fig. 2b), the kinematic and photometric major axes actually deflect in opposite directions from the line of nodes—this is a breakdown of the circular pattern of rotation induced by the bar. However, at $R = 4″$–$6″$, where the star formation ring is located, the orientations of the kinematic and photometric major axes coincide. If we analyzed only the photometric data, then we would unequivocally interpret such a behavior of $PA(R)$ in the ring region as the star formation ring being elliptical in the galactic plane: both observations (Buta and Crocker 1993) and theory (Heller and Shlosman 1996) suggest that the nuclear star formation rings can be noncircular. However, the coincidence of the kinematic and photometric major axes suggests that there can also be a different possible interpretation: the gaseous ring with ongoing star formation may be just tilted to the galactic plane and rotates together with the young stars quite independently in an axisymmetric bulge potential. In principle, the gas can leave the disk plane near the inner Lindblad resonances of the bar, as predicted by some of the theoretical models (see, e.g., Friedli and Benz 1993). In the context of this hypothesis, if the gas at $1″$–$3″$ from the nucleus

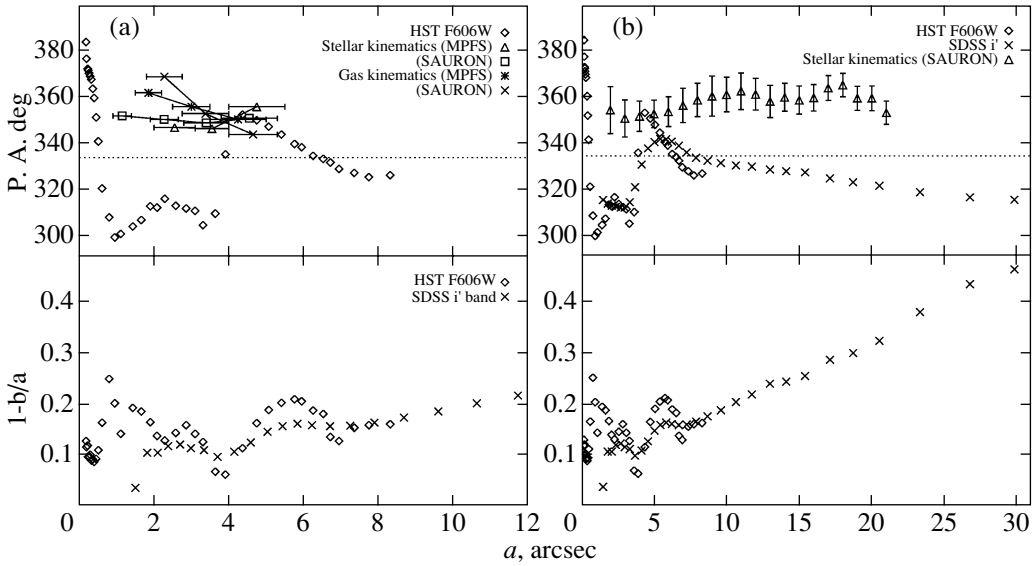

Fig. 2. Top—comparison of the orientations of the photometric and kinematic major axes for the central region of the galaxy under study; the horizontal dotted line indicates the orientation of the line of nodes of the symmetry plane estimated from the outer isophotes belonging to the global galactic stellar disk; bottom—ellipticity of the isophotes from HST (spatial resolution $0''.1$) and SDSS (spatial resolution $1''.3$) images: (a) the innermost region of the galaxy, the kinematic estimates refer to the region of rigid-body rotation and were obtained by searching for a maximum of the apparent line-of-sight velocity gradient, (b) a similar comparison for regions farther from the center, the orientation of the kinematic major axis was determined by the method of tilted rings with the DETKA code of A.V. Moiseev.

is an "inward" extension of the gaseous ring, then the difference between the orientations of the rotation planes can perhaps partly explain the apparent difference between the rotation velocities of the bulge stars and the gas noted above. However, if the rotation plane of the bulge at the center is oriented in the same way as the plane of the outer disk with $i = 40°$, then the maximum possible difference in the line-of-sight projections of the rotation velocities due to the difference between the orientations of the rotation axes will be only $1/\sin i = 1.56$, while a factor of 3 is observed. We can then assume that the true shape of the outer stellar disk is essentially elliptical (which is not surprising, given the dense environment of the galaxy and the presence of an extended "strong" bar) and the galaxy orientation is actually much closer to face-on than at $i = 40°$.

CHARACTERISTICS OF THE STELLAR POPULATION IN THE CENTRAL PART OF NGC 4245

Figure 3, which presents the maps of hydrogen, magnesium, and iron Lick indices constructed from MPFS data for the central region of NGC 4245, clearly shows a chemically decoupled nucleus in this galaxy: both Mg*b* and $\langle \mathrm{Fe} \rangle \equiv (\mathrm{Fe5270} + \mathrm{Fe5335})/2$ maps have a significant, compact central peak. On the Hβ map, the deep minima at $4''$–$5''$ to the northeast and the south of the nucleus mirror the Hα emission maxima (Fig. 1d). This means that the Hβ absorption line is significantly flooded with emission and to use the Lick index Hβ to estimate the stellar population parameters, it should first be corrected for the emission. We will do this using two independent methods.

The first method is based on spectroscopic data for the Hα emission line. This method usually yields proper results, since there exist physical models for the relationship between the Hα and Hβ emission intensities and since the intensity of the Hα emission always exceeds that of the Hβ emission by a factor of several, while the equivalent width of the Hβ absorption line is always of the order of or even larger than that of the Hα absorption line. The smallest Hα/Hβ emission ratio, 2.5–2.7 (Burgess 1958), is obtained in the case of hydrogen excitation (ionization) by ultraviolet radiation from young massive stars (H II-region-type excitation). In active galactic nuclei and at shock fronts, this ratio is even larger; it also increases in the presence of dust in the emitting region. The observational statistics, including the spectra of spiral galaxies with various types of excitation, gives a mean ratio $EW(\mathrm{H}\beta_{\mathrm{emis}}) = 0.25EW(\mathrm{H}\alpha_{\mathrm{emis}})$ (Stasinska and Sodré 2001). Therefore, correcting the index Hβ for the emission in the central region of NGC 4245, we will take $EW(\mathrm{H}\beta_{\mathrm{emis}}) = 0.25EW(\mathrm{H}\alpha_{\mathrm{emis}})$ in the nucleus and $EW(\mathrm{H}\beta_{\mathrm{emis}}) = 0.37EW(\mathrm{H}\alpha_{\mathrm{emis}})$ in the

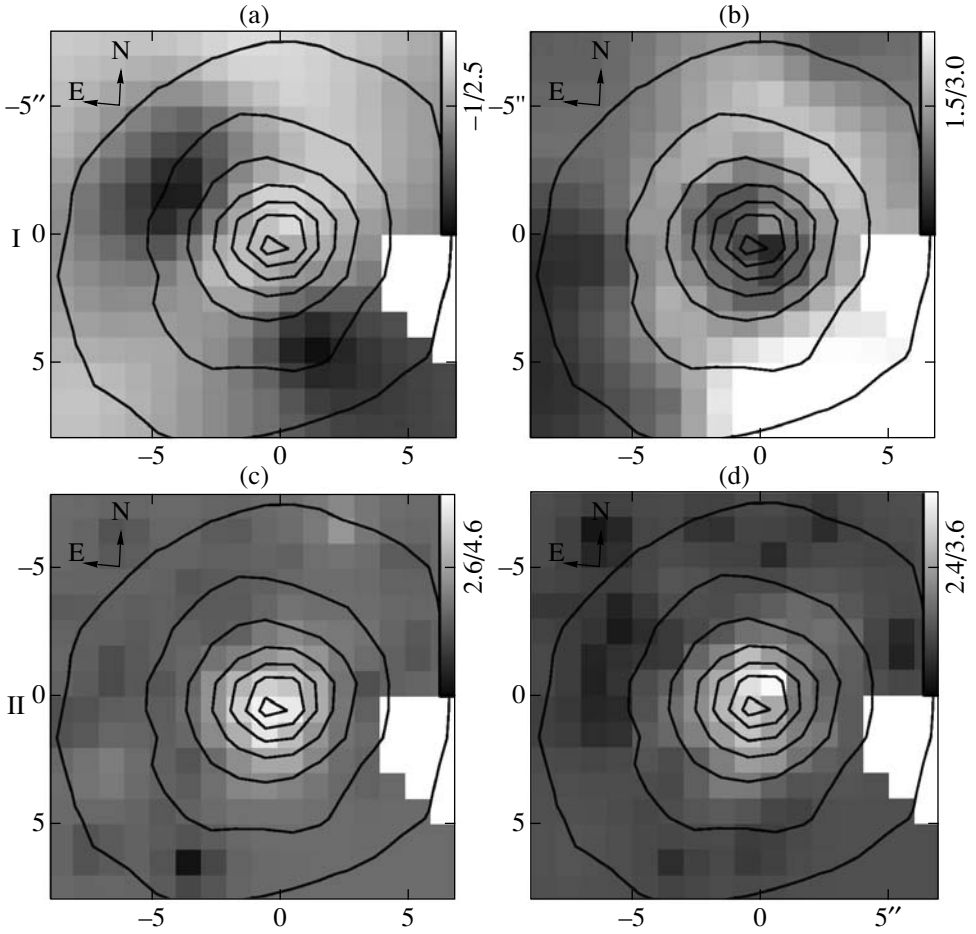

Fig. 3. Maps of Lick indices (in Å) obtained for the central region of NGC 4245 with the MPFS of the 6-m SAO telescope: I—the index Hβ uncorrected (a) and corrected (b) for the contribution from the emission by the second method discussed here; II—the indices Mg*b* (c) and ⟨Fe⟩ (d); the isophotes superimposed on the maps indicate the continuum brightness distribution.

star formation ring ($R = 4''$–$6''$). Since the emission lines in the spectrum of NGC 4245 essentially vanish at $7''$ from the nucleus, we do not correct the Lick index Hβ in the bulge, $R = 7''$–$9''$, for the emission.

The second method consists in fitting the stellar population with model spectra. Since the galaxy spectrum everywhere contains unresolved blends of absorption lines, information about the age and metallicity of the stellar population is contained in each pixel of the spectrum, although the concentration of this information near strong lines is higher than that on average over the spectrum by a factor of several (for the metallicity near strong metal lines and for the age near Balmer lines). Directly fitting the spectra, when each pixel is used to estimate the parameters, allows narrow regions flooded with emission lines to be "cut out" without considerable damage to the quality of the parameter determination. We showed (Chilingarian et al. 2007, 2008) that excluding the Hβ line from the fitting procedure causes no bias of the age estimates. Thus, to calculate the Lick index Hβ, we can reconstruct the fluxes in the central part of the absorption line using values from the model stellar population spectra. In this case, of course, the index can be shifted toward the model values. However, since (a) not the entire range used in determining the index is replaced and (b) the pseudo-continuum regions remain without any changes, the method can be trusted.

Both correction methods provide excellent agreement in the region $R = 1''$–$3''$. In the galactic nucleus and the star formation ring, the second method gives lower estimates of the index than the first method, which we can interpret as enhanced dust absorption inside the galaxy, so that the Hα/Hβ ratio turns out to be higher. In contrast, in the bulge, the correction using model stellar population spectra gives higher values than the method using Hα. This may be the result of residual emissions in Hβ that cannot be detected without subtracting the model stellar population spectrum.

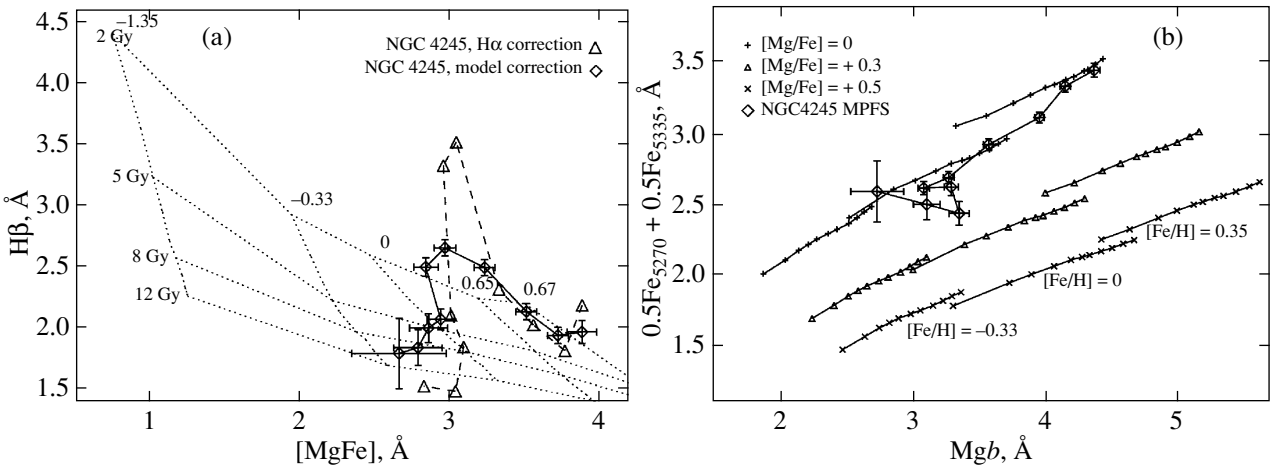

Fig. 4. Diagnostic index–index diagrams for the azimuthally averaged measurements of the Lick indices in the central region of NGC 4245 based on MPFS data: (a) the diagram that compares the combined metal line index (see the text) and the Balmer absorption line index Hβ to diagnose the stellar population age. The large symbols connected by the broken line represent the azimuthally averaged measurements of the indices in NGC 4245 taken along the radius at 1″ steps; the Hβ measurements corrected for the emission by the two methods as described in the text are shown. The observational data are compared with the models from Thomas et al. (2003); the model equal-age and equal-metallicity sequences are marked by $T = 2, 5, 8, 12$ Gyr and [Z/H]= +0.67, +0.3, 0.0, −0.33, −1.35. (b) The diagram that compares the combined iron index (see the text) and the magnesium index to diagnose the magnesium-to-iron abundance ratio for the stellar population. The large symbols connected by the broken line represent the azimuthally averaged measurements of the indices in the galaxy taken along the radius at 1″ steps. The models from Thomas et al. (2003) for three ratios, [Mg/Fe]= 0.0, +0.3, and +0.5 dex, if the "triples" of curves are taken from the top down, are also plotted on the diagram. In each triple for fixed [Mg/Fe], we show the lines of equal metallicity for its three values, −0.33, 0.00, and +0.35 dex, along which the age changes from 3 to 12 Gyr (from left to right).

Figure 4 shows the diagnostic diagrams that allow the mean metallicity, age, and magnesium-to-iron abundance ratio for the stellar population to be determined by comparing one Lick index with another (or a combination of other indices). The index Hβ here has already been corrected for the emission and characterizes the integral spectrum of the purely stellar component. We compare our measurements for NGC 4245 with the synthetic evolutionary models of "simple stellar populations" from Thomas et al. (2003). "Simple" means that each model represents a set of stars of the same age and chemical composition; comparing the integral spectra of real, possibly, inhomogeneous stellar systems with these models, we determine the mean (luminosity-weighted) stellar population parameters. Thomas et al. (2003) constructed their models for several magnesium-to-iron abundance ratios; Fig. 4 shows model equal-age sequences for two values of [Mg/Fe], 0.0 and +0.3. In particular, we see that comparing the index Hβ with the combined metal index $[\mathrm{MgFe}] \equiv (\mathrm{Mg}b\langle\mathrm{Fe}\rangle)^{1/2}$, we get rid of the dependence of the age estimates on the adopted magnesium-to-iron abundance ratio. Comparison of the Lick indices averaged in rings with a sliding radius for NGC 4245 with the models from Thomas et al. (2003) in Fig. 4a indicates that the stellar metallicity in the nucleus is very high, a factor of 3–5 higher than the solar one, while the stellar age is a middle one, 2–4 Gyr. The ring with a radius of $R = 4''$–$5''$ with ongoing star formation is characterized by a mean age of about 1–2 Gyr; this should suggest that star formation has been going on for a long time, at least several hundred Myr, or starbursts have occurred repeatedly in this place of the bulge. When going outside the outer boundary of the star formation ring, we obviously fall into the bulge region: the mean stellar metallicity there is lower than the solar one, while the mean age is about 8–12 Gyr. Given the mean age of the stellar population, the magnesium-to-iron abundance ratio, which is an indicator of the duration of main star formation, can be estimated from the plot in Fig. 4b. In the nucleus, the ring, and the bulge, this ratio does not exceed $[\mathrm{Mg/Fe}] \approx +0.1$. Such a nearly solar ratio again suggests that star formation at the center of NGC 4245 had been going on for at least 2 Gyr; in the ring, it goes on even now.

An important point concerning the technique of calculating the Lick indices is related to the reduction of the measured (instrumental) values to the Lick system used to construct the stellar population models. Several authors, for example, Kuntschner (2004) and Peletier et al. (2007), believe that before the calculation of the indices, the spectral resolution of the data should be artificially degraded to the Lick values by also taking into account the internal stellar velocity

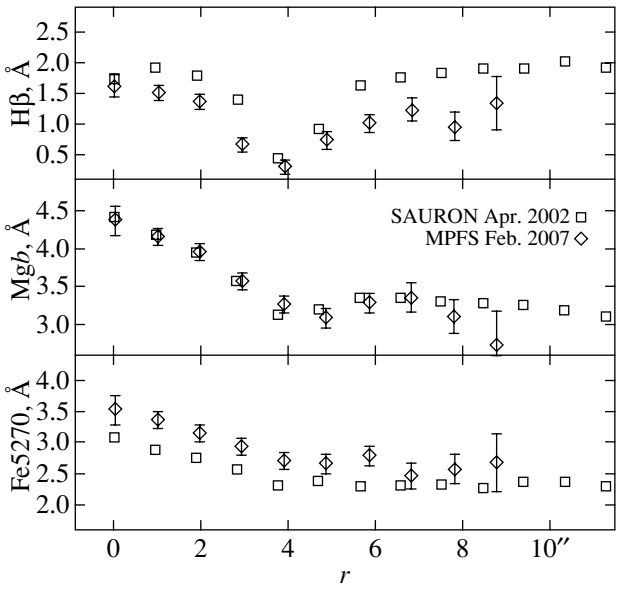

Fig. 5. Comparison of the azimuthally averaged profiles for the Lick indices in the central region of NGC 4245 based on MPFS and SAURON data. This plot shows the initially measured indices Hβ uncorrected for the emission.

dispersion in the galaxy as a physical phenomenon that naturally degrades the spectral resolution (increases the absorption line width). Another approach (e.g., Sil'chenko 2006) consists in a purely empirical transformation of the instrumental indices to the Lick system based on the observations of stars from the Lick library of spectra with the same instrument and in the same mode in which the galaxies were observed. Whereas the index Hβ is not strongly subjected to the spectral resolution effects, the indices Mg*b* and $\langle$Fe$\rangle$ calculated using these two approaches differ by almost 0.4 Å. Therefore, the metallicity obtained by inverting the diagnostic diagrams differs by almost 0.3 dex (the higher metallicity corresponds to the second index transformation method).

Comparison of the metallicities that correspond to the Lick indices calculated by the two methods with those obtained independently by direct fitting reveals good agreement of the direct fitting results with the empirical (second) method that we use (the metallicity difference is only about 0.05 dex).

We also analyzed the integral-field spectroscopy obtained for NGC 4245 by the SAURON team with the William Herschel 4.2-m telescope to estimate the stellar population parameters. Unfortunately, using the Lick indices calculated from SAURON data should be limited mainly to a qualitative analysis: since the spectral range is too narrow, 4800–5350 Å, the standard Lick bands to measure the continuum fall on the transmission cutoff of the instrumentation on the blue side for Hβ and on the red side for Fe5270 and the Hβ and Fe5270 estimates in the galaxy are found to be systematically shifted because of this and because the galaxy has an appreciable redshift with respect to the Lick standard stars. In Fig. 5, we compare the radial variations of the Lick indices averaged in rings based on MPFS and SAURON data. Whereas the Mg*b* measurements in the middle of the range of SAURON observations agree satisfactorily, the values of Hβ obtained from SAURON data are overestimated by 0.3–0.5 Å, while the values of Fe5270 are underestimated approximately by 0.5 Å. We found similar systematic shifts of the Hβ and Fe5270 measurements based on SAURON data when investigating the galaxy NGC 3384 (Sil'chenko et al. 2003) observed with SAURON in March 2000. Obviously, this is a stable feature of the data obtained with this instrumentation and the quantitative data for the Lick indices calculated from SAURON spectra are inevitably shifted systematically. However, qualitatively, the shapes of the radial Hβ and Fe5270 profiles based on MPFS and SAURON data agree well and it is natural to analyze the morphology of the surface distribution of Lick indices using SAURON data as well.

To obtain quantitative estimates of the stellar population parameters from SAURON data, we applied a channel-by-channel direct spectrum fitting procedure to the data cube processed by the SAURON team, just as to the MPFS data, by simultaneously varying the age, metallicity, and kinematic parameters of the stellar component (Chilingarian et al. 2007). Since this method is based on the ELODIE library of observed spectra for bright (mostly nearby) stars, a solar magnesium-to-iron ratio is implied, which corresponds to the actual situation for

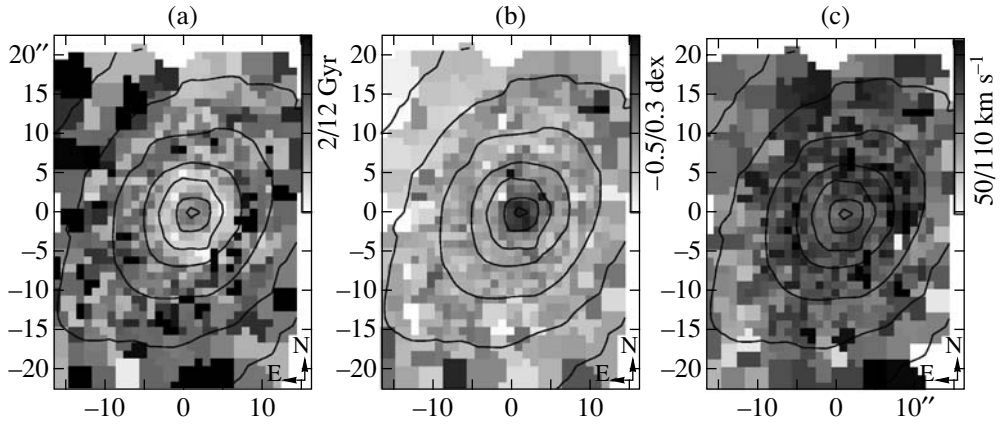

Fig. 6. Maps of stellar population parameters obtained for the central region of NGC 4245 from SAURON data by directly fitting the spectra: from left to right, the mean age, in Gyr, mean metallicity, on a logarithmic scale with respect to the Sun, and stellar velocity dispersion, in km s^{-1} (the gray scales on the right side of each panel).

NGC 4245. Figure 6 presents the stellar metallicity, age, and velocity dispersion maps that we obtained from the SAURON data cube by this method. Qualitatively, the results completely agree with those obtained from MPFS data using Lick indices: we see a compact, chemically decoupled nucleus, a young ring with a radius of 4″–5″, and a minimum of the stellar velocity dispersion in the nucleus. In contrast, quantitatively, we obtained estimates slightly different from those based on MPFS data: the metallicity and the mean stellar age in the nucleus are [m/H] = +0.2 and 6.5 Gyr, respectively, the mean stellar age in the ring is 4 Gyr (in some knots, 2 Gyr), and the metallicity and the mean stellar age in the bulge ($R = 7''$–$9''$) are [m/H] = −0.2 and 8 Gyr, respectively. Interestingly, in contrast to the Lick indices, the channel-by-channel spectrum fitting method showed no increase in mean stellar metallicity in the star formation ring. This can be only if star formation in the ring began quite recently. Thus, the duration of star formation in the ring cannot yet be estimated unambiguously.

It is worth noting that the models by Thomas et al. (2003) are based on the Lick library of stellar spectra. At the same time, the ELODIE.3 library, on which the PEGASE.HR models are based, has a much fuller coverage of the space of physical parameters (effective temperature and surface gravity), especially for low- and high-metallicity stars. Therefore, the absolute age estimates for young and middle-aged (up to 3 Gyr) stellar populations based on the PEGASE.HR models should be trusted more than the estimates from the models by Thomas et al. (2003). This conclusion is applicable mainly to the inner ring of young stars, since the mean metallicity of the stellar population there is rather high.

DISCUSSION

The (circum)nuclear star formation rings are traditionally linked to the inner Lindblad resonances of a bar rotating in the galactic disk. The extensive statistics of metric ring sizes collected by Buta and Crocker (1993) allowed them to establish this link empirically. Subsequently, dynamical modeling of the response of the galactic disk gas to a rotating bar allowed one to confirm that this link is physically justified and to outline some of the morphological and evolutionary features of the star formation rings (see, e.g., Heller and Shlosman 1996). In the object of our investigation, NGC 4245, the circumnuclear star formation ring shows all classical signatures. In Fig. 7, we determine the positions of the inner Lindblad resonances associated with the large-scale bar of NGC 4245. In this case, we use the rotation curve of the stellar component constructed by a cut along the major axis over the SAURON velocity field and fitted by a fourth-degree polynomial and the bar pattern speed determined kinematically by Treuthardt et al. (2007) from the apparent stellar line-of-sight velocity distribution by the method of Tremaine and Weinberg (1984), 75.5 ± 31.1 km s^{-1} kpc^{-1}. We see that at a fixed pattern speed, given its uncertainty, the bar can have two inner Lindblad resonances, approximately at the positions $R_{\rm iilr} = 4.8''$ and $R_{\rm oilr} = 5.8''$; the fixed pattern speed has such an accuracy that these positions can be shifted: the inner inner one to $R_{\rm iilr} = 2''$ and the outer inner one to $R_{\rm oilr} = 9''$. Thus, the star formation ring falls exactly between the two inner Lindblad resonances, as predicted by the theory (see, e.g., Heller and Shlosman 1996).

Figure 8 presents the complete $g' - i'$ color map for NGC 4245 that we calculated from SDSS data; the colors were reduced to the absolute scale with

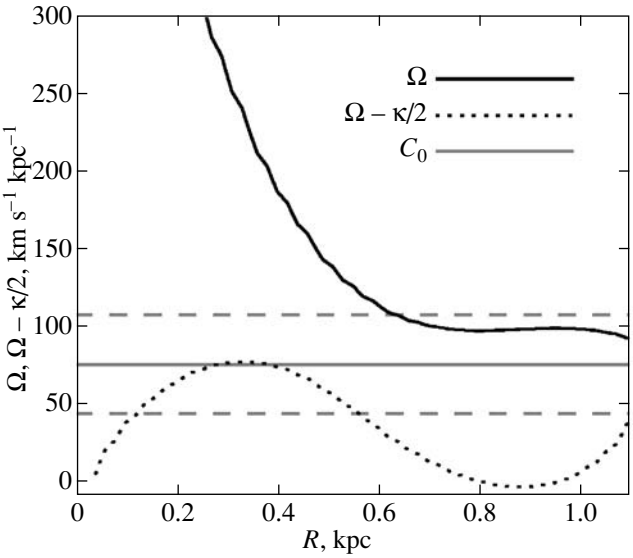

Fig. 7. Curve of the angular velocity of stellar rotation in the central region of NGC 4245 based on SAURON data and positions of the inner Lindblad resonances; the bar pattern speed was taken from Treuthardt et al. (2007), the dashed horizontal lines indicate the interval of uncertainty in their estimate.

the standard technique of correction for the atmosphere; no correction for the extinction inside the Galaxy was applied (in any case, it is no more than $0^m.03$). To exclude the appearance of artifacts, we reduced the images to a spatial resolution of $1''.8''$ before constructing the color map. To accurately determine the colors in the outer parts of the galaxy, we used adaptive Voronoi tesseleration (Cappellari and Copin 2003) for a minimum signal-to-noise ratio of 80 in g'.

Here, the large-scale bar of the galaxy also shows classical signatures predicted by dynamical models: straight thin red (dust) lanes that outline the shock fronts where the gas (associated with dust) "clusters", because the orbits turn in a triaxial potential, stretch over the edges of the bar along its entire length (see, e.g., Athanassoula 1992). The dust fronts end at the circumnuclear star formation ring, which stands out by its blueness on the color map. Three particularly blue knots whose positions coincide with those of the Hα emission knots can be seen in the ring (Fig. 1d)—obviously, these are the sites of the most intense current star formation. Two of these three knots lie exactly at the locations where the dust fronts encounter the ring. This picture, which has already been pointed out in barred galaxies (see, e.g., Boker et al. 2008), is interpreted by theorists as evidence that the gas from the outer galactic disk regions flows down exactly along the bar edges into the ring; at the locations where the radial gas flows encounter the ring, the shock wave is particularly strong and it is here that a local starburst that subsequently is "smeared" into the ring is triggered. According to the theory, the gas will not flow down deeper than the inner inner Lindblad resonance and this is a long formulated problem for the fueling of active galactic nuclei: How can the gas be "shaken off" from a radius of $\sim$1 kpc to a radius of $\sim$1 pc? To solve this problem, theorists proposed three types of dynamical mechanisms (Combes 2001): $m = 2$ gaseous disk perturbations (a bar or a two-arm spiral), $m = 1$ gaseous disk perturbations (lopsidedness or a one-arm spiral), and gaseous disk perturbations by an external tidal impact. Futile attempts to confirm the latter mechanism by the observational statistics of the coincidence of the presence of an active nucleus and the presence of a perturbing "neighbor" have been made for more than one decade. Theorists develop mainly the first class of mechanisms: we known the AGN fueling models by Shlosman et al. (1989) for compact nested "secondary" bars and the models of nuclear spirals in the gaseous disk by Maciejewski (2004a, 2004b).

Our investigation of the central region of NGC 4245 shows that at least in the past, the gas overcame the inner Lindblad resonance in its onflow along the bar: the nucleus within $1''$–$2''$ is chemically decoupled and the mean stellar age in the nucleus is younger than that on average in the bulge. This means that there was a secondary starburst in the nucleus several Gyr ago and this required delivering a gas there. We and the SAURON team are now observing its remnants at the galactic center in the Hα, [N II] λ6583, and [O III] λ5007 emission lines. However, curiously enough, this starburst seems to have been not a "nuclear" but a "ring" one. HST observations showed that within $0''.25$ of the center (an unattainable spatial resolution for the MPFS and

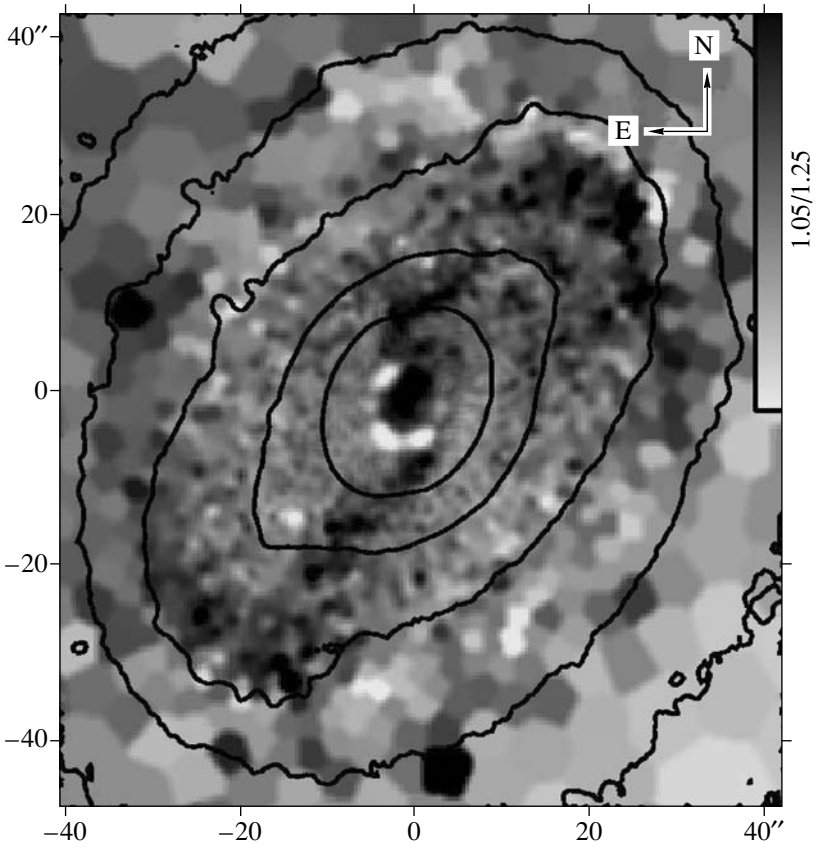

Fig. 8. $(g' - i')$ color map for NGC 4245 calculated from SDSS data. The isophotes superimposed on the map indicate the continuum surface brightness distribution in g'.

SAURON!), the emissions are completely absent and the stellar population is older than 10 Gyr, with the possible presence of no more than 1% of a younger stellar population (Shields et al. 2007; Sarzi et al. 2005). This means that the starburst that produced the chemically decoupled stellar nucleus we found actually occurred outside $0''.25$ (12–15 pc); obviously, the gas has never reached the very center over the lifetime of the galaxy. This suggests that a compact "nuclear" (secondary) bar with the inner Lindblad resonance at $R = 0''.5$–$1''$ could exist in the past at the center of NGC 4245. The "relic" evidence for the existence of such a bar in the past is a great turn of the photometric major axis in the range $R = 1''$–$3''$ to $PA \approx 300°$–$310°$, although the low ellipticity of the isophotes prevents us from recognizing the presence of a *current* nuclear minibar at this location. It was in the past but later dispersed, leaving only the "lens" behind and the circumnuclear star formation ring moved from $R = 0''.5$–$1''$ to the current position $R = 4''$–$5''$. So far the dynamical models reconstruct the secondary bars only in transient mode, which is consistent with our hypothesis. The currently observed remnant from the former star formation ring, the chemically decoupled nucleus, can probably attributed to the class of the so-called ultracompact nuclear star formation rings with a radius of less than 150 pc, which have been discovered just recently in galaxies with bars and oval lenses and only a few of which are known to date (Comerón et al. 2008).

ACKNOWLEDGMENTS

We wish to thank A.V. Moiseev, a senior researcher from the Special Astrophysical Observatory of the Russian Academy of Sciences, for support of the MPFS observations on the 6-m telescope and analysis of the stellar velocity field in NGC 4245 with the SAURON spectrograph using the DETKA code. We used observational data from the William Herschel telescope on the La Palma island operated by the Royal Greenwich Observatory at the del Roque de los Muchachos Spanish Observatory of the Institute for Astrophysics of the Canary Islands and taken from the publicly accessible Isaac Newton Group archive at the Astronomical Data Center of Great Britain; we are grateful to Jesus Falcon-Barroso who provided the processed SAURON data cube for NGC 4245. We also used data from the NASA/ESA Hubble

Space Telescope operated by the Association of Universities for Research in Astronomy under contract with NASA, NAS 5-26555, and SDSS photometric data. During our work, we relied on the means of HYPERLEDA, the Lyon–Meudon Extragalactic Database, provided by the LEDA team at the Lyon CRAL Observatory (France) and the NASA/IPAC database (NED) operated by the Jet Propulsion Laboratory of the California Institute of Technology under contract NASA. This work was supported by the Russian Foundation for Basic Research (project no. 07-02-00229a).

REFERENCES

1. E. Athanassoula, Mon. Not. R. Astron. Soc. **259**, 345 (1992).
2. V. L. Afanasiev, S. N. Dodonov, and A. V. Moiseev, *Stellar Dynamics: from Classic to Modern* (Ed. by L. P. Osipkov, I. I. Nikiforov, St.-Pb. State Univ., St. Petersburg, 2001), p. 103.
3. R. Bacon, Y. Copin, G. Monnet, et al., Mon. Not. R. Astron. Soc. **326**, 23 (2001).
4. T. Boker, J. Falcon-Barroso, E. Schinnerer, et al., Astron. J. **135**, 479 (2008).
5. A. Burgess, Mon. Not. R. Astron. Soc. **118**, 477 (1958).
6. R. Buta and D. A. Crocker, Astron. J. **105**, 1344 (1993).
7. M. Cappellari and Y. Copin, Mon. Not. R. Astron. Soc. **342**, 345 (2003).
8. I. V. Chilingarian, P. Prugniel, O. K. Sil'chenko, and V. L. Afanasiev, Mon. Not. R. Astron. Soc. **376**, 1033 (2007).
9. I. V. Chilingarian, V. Cayatte, F. Durret, et al., Astron. Astrophys. **486**, 85 (2008).
10. F. Combes, *Advanced Lectures on the Starburst-AGN Connection*, Ed. by I. Aretxaga, D. Kunth, and R. Mújica (World Sci., Singapore, 2001), p. 223.
11. S. Comerón, J. H. Knapen, J. E. Beckman, and I. Shlosman, Astron. Astrophys. **478**, 403 (2008).
12. J. Falcon-Barroso, R. Bacon, M. Bureau, et al., Mon. Not. R. Astron. Soc. **369**, 529 (2006).
13. D. Friedli and W. Benz, Astron. Astrophys. **268**, 65 (1993).
14. M. Gerin and F. Casoli, Astron. Astrophys. **290**, 49 (1994).
15. J. A. Garcia-Barreto, D. Downes, and W. K. Huchtmeier, Astron. Astrophys. **288**, 705 (1994).
16. S. A. Gregory and L. A. Thompson, Astrophys. J. **213**, 345 (1977).
17. C. H. Heller and I. Shlosman, Astrophys. J. **471**, 143 (1996).
18. J. D. Kenney and J. S. Young, Astrophys. J. **301**, L13 (1986).
19. J. Kormendy and R. C. Kennicutt, Jr., Ann. Rev. Astron. Astrophys. **42**, 603 (2004).
20. H. Kuntschner, Astron. Astrophys. **426**, 737 (2004).
21. D. Le Borgne, B. Rocca-Volmerange, P. Prugniel, et al., Astron. Astrophys. **425**, 881 (2004).
22. W. Maciejewski, Mon. Not. R. Astron. Soc. **354**, 883 (2004a).
23. W. Maciejewski, Mon. Not. R. Astron. Soc. **354**, 892 (2004b).
24. A. V. Moiseev and V. V. Muscevoĭ, Pis'ma Astron. Zh. **26**, 657 (2000) [Astron. Lett. **26**, 565 (2000)].
25. J. S. Mulchaey, D. S. Davis, R. F. Mushotsky, and D. Burstein, Astrophys. J. Suppl. Ser. **145**, 39 (2003).
26. R. F. Peletier, J. Falcon-Barroso, R. Bacon, et al., Mon. Not. R. Astron. Soc. **379**, 445 (2007).
27. P. Prugniel and C. Soubiran, astro-ph/0409214 (2004).
28. M. Sarzi, H.-W. Rix, J. C. Shields, et al., Astrophys. J. **628**, 169 (2005).
29. J. C. Shields, H.-W. Rix, M. Sarzi, et al., Astrophys. J. **654**, 125 (2007).
30. I. Shlosman, J. Frank, and M. C. Begelman, Nature **338**, 45 (1989).
31. O. K. Sil'chenko, A. V. Moiseev, V. L. Afanasiev, et al., Astrophys. J. **591**, 185 (2003).
32. O. K. Sil'chenko, Astrophys. J. **641**, 229 (2006).
33. J. M. Solanes, A. Manrique, C. Garcia-Gomez, et al., Astrophys. J. **548**, 97 (2001).
34. G. Stasinska and I. Sodré, Jr., Astron. Astrophys. **374**, 919 (2001).
35. W. T. Sullivan III and P. E. Johnson, Astrophys. J. **225**, 751 (1978).
36. D. Thomas, C. Maraston, and R. Bender, Mon. Not. R. Astron. Soc. **339**, 897 (2003).
37. P. Treuthardt, R. Buta, H. Salo, and E. Laurikainen, Astron. J. **134**, 1195 (2007).
38. S. Tremaine and M. D. Weinberg, Astrophys. J. **282**, L5 (1984).
39. G. Worthey, Astrophys. J. Suppl. Ser. **95**, 107 (1994).
40. G. Worthey, S. M. Faber, J. J. Gonzalez, and D. Burstein, Astrophys. J. Suppl. Ser. **94**, 687 (1994).

Translated by V. Astakhov